Advances in Nano Research, *Vol. 18, No. 6 (2025) 549-564*
https://doi.org/10.12989/anr.2025.18.6.549

Vibration analysis of viscoelastic functionally graded porous nanoshell

Mehmet Bugra Özbey[a] and Faruk Firat Calim[*]

Department of Civil Engineering, Adana Alparslan Turkes Science and Technology University, Adana, Türkiye

(*Received November 6, 2024, Revised March 22, 2025, Accepted March 24, 2025*)

Abstract. This paper presents dynamic analyses for nanoscale shells with various geometries, utilizing linear standard viscoelastic material properties and functionally graded porous materials. The displacements in Cartesian coordinates for FG porous nanoshell are formulated utilizing a stress and strain shape function based on higher order shear deformation theory, which has been previously employed in the literature. The motion's equations are derived through Hamilton principle, incorporating energy expressions of the system. The forces and moments in motion's equations are expressed with nonlocal terms based on Eringen's nonlocal elasticity theory. Navier method, which allows analytical solutions for simply supported conditions, is employed in the analysis. For the dynamic analysis, dynamic distributed load applied to nanoshell is represented as a trigonometric series. To facilitate the solution, displacements are obtained in Laplace domain and subsequently transformed back into time domain. Material properties in the analysis are represented employing linear standard viscoelastic model. In this context, a computational method is developed utilizing Mathematica, and its accuracy is validated by performing a free vibration analysis. The obtained natural frequencies are compared with values from previous studies in the literature to demonstrate the model's reliability. Subsequently, a series of forced vibration analyses are conducted under dynamic distributed loading as part of parametric study on functionally graded porous viscoelastic nanoshell. The influences of different geometries, geometric properties, nanoscale characteristics, material variations, linear standard viscoelastic coefficients, porosity distributions, and porosity on displacements are investigated.

Keywords: Eringen's nonlocal elasticity theory; functionally graded material; linear standard viscoelastic model; nanoshell; porous distribution

1. Introduction

Nanostructures are systems with one or more dimensions at the nanoscale. When structures are at nanoscale, they can exhibit distinct optical, mechanical, and electrical properties compared to their larger-scale counterparts. Nanoscale technology allows achieving desired performance with less material. Moreover, it enables the creation of high-performance, lighter, stronger, and more durable structures. Although relatively new, nano-structures are being used in the construction engineering sector for insulation technologies, roofing and facade coatings, and within load-bearing concrete systems. In addition, their exceptional magnetic, optical, and electronic properties make them highly applicable in fields such as healthcare, textiles, industry, and defence. Nano-technology is frequently utilized in sensors, optical and communication devices, print heads, and solar cells (Farajpour *et al*. 2018, Karami *et al*. 2019, Mehralian *et al*. 2016). Functionally graded materials (FGMs) are hetero-geneous materials in which properties are gradually varied in a controlled manner through the thickness. This concept was first introduced by Japanese scientists in the mid-1980s. FGMs are typically composed of a combination of metals and ceramics, leveraging the heat and corrosion resistance of ceramics along with the high tensile strength of metals. FGMs are particularly useful in applications like space shuttle tiles, where ductility is needed on the inner side and extreme temperature resistance on the outer side. The material properties in FGMs continuously change, eliminating interfaces between different materials and thus mitigating issues related to material discontinuity, such as delamination failure (Ghayesh and Farajpour 2019, Karami and Janghorban 2020, Kiani *et al*. 2012a, b, Wang *et al*. 2023). Porous materials, known for their lightweight characteristics, are widely utilized in the aerospace industry and hold significant importance in the literature. Additionally, due to imperfections in the manufacturing process, voids can naturally form within the materials. Therefore, analysing the effects of porosity on mechanical properties is crucial (Faleh *et al*. 2018, Civalek *et al*. 2023, Addou *et al*. 2024). For all these reasons, numerous studies in the literature focus on functionally graded materials, porosity, and nanoscale properties.

Altenbach and Eremeyev (2011) highlighted surface stresses' influence, which are essential in nanoscale structure such as nanofilm and nanoporous materials, demonstrating how these effects alter material stiffness and behaviour at the nano level. Ghadiri and Safarpour (2016) analysed the influence of material length scale, temperature variations, electrical and magnetic potentials, and shear correction factor on the natural frequencies of nanoshell subjected to combined thermo-electro-magnetic loadings with simply supported boundary conditions. Rouhi *et al*.

*Corresponding author, Professor,
E-mail: ffcalim@atu.edu.tr
[a] Ph.D. Student, E-mail: mbozbey@atu.edu.tr

ISSN: 2287-237X (Print), 2287-2388 (Online)

(2016) investigated how surface characteristics, including elastic moduli and surface tension, impact nanoshells' vibrational performance, particularly highlighting that surface stresses play a pivotal role in altering the resonant frequencies, especially in thin structures. Sahmani *et al*. (2016) conducted novel investigation into cylindrical nanoshells' nonlinear post-buckling response, incorporating surface stress impacts for the first time. Also, they examined how surface elasticity and residual surface stress influence both the critical buckling load and end-shortening in silicon nanoshells. Zhao *et al*. (2018) synthesized a novel porous metal-organic framework with uncoordinated O donor sites and investigated its potential for 5-fluorouracil loading, analysing drug-loading capacity, pH-sensitive release, and cytotoxicity against MG63. Mirjavadi *et al*. (2020) explored forced vibration response of porosity dependent functionally graded cylindrical nanoshells subjected to linear or triangular impulse loads. They examined how transient response are influenced by the shape and position of the impulse load, as well as by porosity levels, distribution, and nonlocal and strain gradient factors. Arefi (2020) introduced free vibration behaviour's innovative analysis of doubly curved piezoelectric nanoshells on Pasternak foundation, considering the integrated impacts of initial electro-mechanical loads, advanced shear deformation theory, and nonlocal elasticity. Kachapi (2020) examined how piezoelectric nanoshell's natural frequencies and nonlinear responses vary under electrostatic voltage, different loading conditions, nanoscale effects, and interface properties. Eyvazian *et al*. (2020) examined how various factors such as size-dependent effects, weight ratio, number of GNP layers, elastic foundation characteristics, and excitation frequency influence functionally graded graphene nanoplatelets-reinforced composite cylindrical nanoshell's forced vibration response. Their study, which also accounts for changes in load velocity and time history, provided insights into nanoshell's dynamic response under moving harmonic loads. Dai and Safarpour (2021) examined how doubly curved laminated nanoshell's thermal buckling and natural frequency vary with geometric and material properties. Xu *et al*. (2021) incorporated the nonlocal stain gradient theory to account for nano scale impacts and analysed various nanoshell geometries, examining the influence of parameters such as porosity, material gradient, and elastic foundation to nanoshell's dynamic response. Cao *et al*. (2021) addressed the mechanical response of three-dimensional functionally graded (FG) nanoshells and nanoplates for the first time. They investigated how nanoscale properties, variations in material characteristics, and different geometrical shapes affected natural frequencies. Vinh and Tounsi (2022) investigated FG doubly curved nanoshells' free vibration response by incorporating a modified nonlocal elasticity theory with varying nonlocal parameters, addressing a gap in previous studies that assumed constant nonlocal parameters, while also investigating the impacts of geometric properties and material gradation. Monge *et al*. (2023) introduced novel semi-analytical 3D approach for FG nanoshell that incorporates the nano-scale effects derived from Eringen's nonlocal elasticity theory. Their study focused on examining how curvature radii and various loading conditions affect the response of both isotropic and FG nanoshells. Thang *et al*. (2023) explored the influence of nonlocal and strain gradient factors, as well as varying carbon nanotube distributions, on the deflection and natural frequencies of double-curved functionally graded carbon nanotube reinforced composite nanoshell. Su *et al*. (2023) systematically examined the stress-strain responses, Young's modulus, ultimate tensile strength, and energy dissipation characteristics of sintered silver nanoparticles, highlighting the statistical correlations between porosity distribution and material performance. Vinh *et al*. (2023) utilized Eringen's nonlocal elasticity theory's modified form to explore the impact of changes in material characteristics, geometry, porosity, and nonlocal parameters on nanoshell's the vibration response. Ghazwani *et al*. (2024a) conducted a high-frequency vibration analysis FG sandwich nanobeams on elastic foundations by integrating nonlocal elasticity and quasi-3D theory to capture size-dependent impacts. Ghazwani *et al*. (2024b) analysed free vibration behaviour of FG sandwich nanobeams on elastic foundations utilizing a novel quasi 3D theory, incorporating size-dependent impacts and evaluating the impact of foundation properties. Fang *et al*. (2024) explored how mechanical and thermal loads, along with variations in volume fraction and reinforcement's folding degree, influence nanoshell's natural frequencies under different boundary conditions, applying micromechanical modelling techniques. Cong *et al*. (2024) explored the influence of material length scale, nonlocal factors, and geometric characteristics on the nonlinear vibration response of FG nanoshell supported by Kerr foundation under harmonic loading, employing nonlocal strain gradient theory alongside classical shell theory. Alnujaie *et al*. (2024) analysed novel coated functionally graded graphene reinforced composite nanoplates, investigating the impact of nanoscale effects and various material distributions and properties. Eltaher *et al*. (2024a) investigated the variations in bending deflections and critical buckling loads of doubly curved laminated shell with a novel graphene-based nanocomposite, considering the effects of nanoscale features, graphene reinforcement, and different shell geometries. Eltaher *et al*. (2024b) investigated the influences of reinforcement properties, foundation support, moving point load, geometric characteristics on functionally graded carbon nanotube nanoplates' free and forced vibration responses. Zhang *et al*. (2025a) systematically investigated the impacts of carrier concentration, interface conditions, plate thickness, and bias electric fields on phase velocity dispersion and attenuation characteristics in multilayered piezoelectric semiconductor plates with imperfect interfaces. Zhang *et al*. (2025b) developed MoS_2/BPC composites from bagasse-derived porous carbon utilizing a hydrothermal process and examined how hydrothermal temperature and duration impact structural characteristics, graphitization, chemical composition, and electromagnetic wave absorption. Doan *et al*. (2025) investigated damped vibration response of FG graphene oxide powder-reinforced composite plates on viscoelastic foundations, emphasizing the impacts of graphene oxide distribution and damping parameters on

vibration behaviour. Alam *et al*. (2025) derived closed-form analytical solution for linear and nonlinear frequencies of magneto-electro-elastic composite nano beams resting on a Pasternak-type substrate utilizing HSDT and variational principles, providing insights into the impacts of geometric nonlinearity, long-range molecular interactions, and substrate stiffness. Vinh and Zenkour (2025) investigated damped vibration response of FG sandwich porous plates resting on a visco-Winkler-Pasternak foundation, analysing the impacts of various boundary conditions, porosity, and damping. He *et al*. (2025) investigated the impacts of stiffness, damping ratios, time delay, fractional order, and excitation force on rolling mills' nonlinear vertical vibration. Son *et al*. (2025) analysed the damped vibration response of FG sandwich porous plates on a visco-Winkler-Pasternak foundation, examining the impacts of various boundary conditions, porosity, and damping. Yang *et al*. (2025) examined flexible risers' vortex-induced vibration by integrating the wake-oscillator model with structural motion equations, analysing displacement, dominant mode, dominant frequency, energy conversion, and space time evolution. Babagi *et al*. (2025) proposed a novel set of scalar potential functions to decouple governing equations in the free vibration and stability analysis of simply supported nanoplates utilizing nonlocal elasticity theory. Vinh (2025) analysed FG nanoplates combining the advantages of nonlocal elasticity and strain gradient theories. Özbey and Calim (2025) investigated the dynamic behaviour of FG viscoelastic nanoplates under dynamic loading, considering nonlocal impacts, material gradation, viscoelastic damping, and geometric parameters, while developing an analytical approach for both free and damped forced vibration analysis.

An extensive literature review has identified a gap in research focused on the damped forced vibration analysis of functionally graded (FG) porous nanoshells with double curvature using viscoelastic material models, which provide more realistic results. Notably, there is a lack of studies in the literature that focus on investigating the dynamic behaviour of nanoshells with an emphasis on viscoelastic material properties and functionally graded porous materials. Although elastic vibration models can incorporate damping impacts and offer simpler solutions, viscoelastic models better capture material behaviour due to internal friction, resulting in more accurate outcomes. This study utilizes the linear standard viscoelastic material model to achieve this realism. While displacement fields for nano-shell are derived utilizing higher order shear deformation theory (HSDT), nanoscale impacts are incorporated into the analysis through stresses employing Eringen's nonlocal elasticity theory. The governing motion's equation, formulated with Hamilton's principle involving energy expressions, are solved employing Navier method based on double Fourier series. Displacements are determined in Laplace domain, bypassing time-step selection, and subsequently transformed to the time domain through Durbin's procedure. A new computational method is developed with Mathematica, and its accuracy is confirmed by comparing free vibration analysis results with existing literature. Subsequently, a series of damped forced vibration analyses are performed to investigate FG porous viscoelastic nanoshell's dynamic response. Initially, the influences of various parameters, including the retardation time linked to the relaxation function, porosity, nonlocal, and power law parameters, on FG porous viscoelastic nanoshell's time dependent displacements are examined. Following this, a study focusing on the impact of linear standard viscoelastic material model coefficients (the retardation time linked to the relaxation function and the proportion of the instantaneous value) on FG porous viscoelastic nanoshell's time dependent displacements is conducted. Finally, a series of maximum displacement analyses are carried out to explore the effects of different shell geometries, curvature radii, nanoshell thicknesses, porosity distributions, and the parameters of porosity, nonlocal and power law on FG porous viscoelastic nanoshell's maximum displacements.

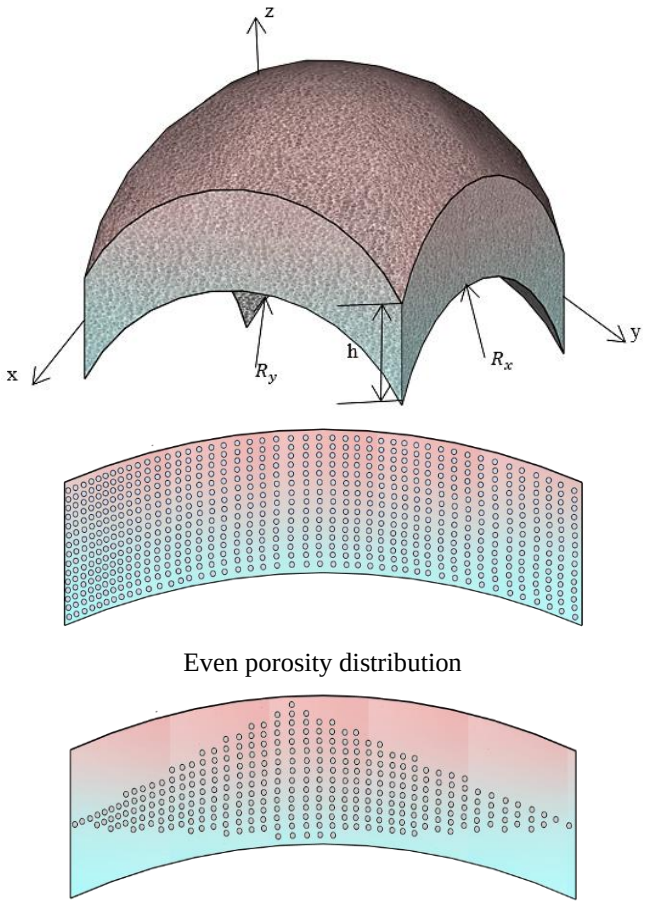

Fig. 1 FG porous viscoelastic nanoshell

2. Formulation

This research focuses on the dynamic performance of simply supported FG viscoelastic nanoshell with porous and defined by dimensions a (length), b (width), and h (thickness), as illustrated in Fig. 1. Nanoshell's geometry varies depending on the radii of curvature in the x and y

directions (R_x, R_y). Specifically, this relationship is defined as $R_x = R_y \neq \infty$ for spherical shell, $R_x \neq \infty$ and $R_y = \infty$ for cylindrical shell and $R_x = R_y = \infty$ for plate.

The upper surface of FG porous nanoshell $(z = h/2)$ is composed of ceramic, while the lower surface $(z = -h/2)$ is made of metal. Within FG porous nanoshell, from $z = -h/2$ to $z = h/2$, material properties (Young's modulus (E), Poisson's ratio(υ), and mass density (ρ)) transition functionally from metal to ceramic. This variation is governed by function $P(z)$ dependent on z coordinate. For even porosity distribution (PI), $P(z)$ function is applied as shown below.

$$P(z) = P_m + (P_c - P_m)\left(\frac{1}{2} + \frac{z}{h}\right)^k - \frac{\xi}{2}(P_c + P_m) \tag{1}$$

In cases where porosity is unevenly distributed (PII) across FG porous nanoshell, the material variation is governed by function $P(z)$, as shown below.

$$P(z) = P_m + (P_c - P_m)\left(\frac{1}{2} + \frac{z}{h}\right)^k - \frac{\xi}{2}(P_c + P_m)\left(1 - \frac{2|z|}{h}\right) \tag{2}$$

k defines power law parameter, controlling the gradual shift from ceramic to metal material properties. The porosity parameter is represented by ξ, which defines the level of voids within the material. The properties denoted by m correspond to the metal, while c represents the ceramic characteristics.

The displacement components in FG nanoshell's x, y and z directions are formulated utilizing HSDT, as demonstrated in the subsequent expressions.

$$\begin{aligned} u &= \left(1 + \tfrac{z}{R_x}\right)u_o - zw_{o,x} + f(z)\,\theta \\ v &= \left(1 + \tfrac{z}{R_y}\right)v_o - zw_{o,y} + f(z)\,\psi \\ w &= w_o \end{aligned} \tag{3}$$

In this context, u_o, v_o, and w_o signify FG nanoshell's the displacements along x, y, and z axis of the central plane, respectively. Rotations around the x and y axes are represented by θ and ψ, respectively. $f(z)$ describes the distribution of deformation and stresses and is formulated utilizing trigonometric shape functions derived from HSDT (Zaoui *et al*. 2019, Calim and Özbey 2023, Rachid *et al*. 2022, Cuma *et al*. 2023).

$$f(z) = \frac{\pi\, h}{\pi^4 + h^4} e^{\left(\frac{hz}{\pi}\right)}\left(\pi^2 sin\left(\frac{\pi z}{h}\right) + h^2 cos\left(\frac{\pi z}{h}\right)\right) - \frac{\pi\, h^3}{\pi^4 + h^4} \tag{4}$$

Utilizing the displacements in Eq. (3) and their derivatives, normal and shear strains for FG nanoshell are derived as follows, based the assumption $\left(1 + (z/R_x)\right) \approx 1$ and $\left(1 + (z/R_y)\right) \approx 1$, which arises from the conditions $h \ll R_x$ and $h \ll R_y$.

$$\begin{aligned} \varepsilon_x &= \frac{\partial u}{\partial x} + \frac{\mathrm{w}_0}{\mathrm{R_x}} = u_{0,x} + \frac{\mathrm{w}_0}{\mathrm{R_x}} - z\, w_{0,xx} + f(z)\,\theta_{,x} \\ \varepsilon_y &= \frac{\partial v}{\partial y} + \frac{\mathrm{w}_0}{\mathrm{R}_y} = v_{0,y} + \frac{\mathrm{w}_0}{\mathrm{R}_y} - z\, w_{0,yy} + f(z)\,\psi_{,y} \\ \gamma_{yz} &= \frac{\partial v}{\partial z} + \frac{\partial w}{\partial y} - \frac{v_0}{\mathrm{R}_y} = f\quad'(z) \\ \gamma_{xz} &= \frac{\partial u}{\partial z} + \frac{\partial w}{\partial x} - \frac{u_0}{\mathrm{R_x}} = f\,'(z)\,\theta \\ \gamma_{xy} &= \frac{\partial u}{\partial y} + \frac{\partial v}{\partial x} = u_{0,y} + v_{0,x} - 2z\, w_{0,xy} + f(z)\,(\theta_{,y} + \psi_{,x}) \end{aligned} \tag{5}$$

Considering nanoshell's thickness, it is observed that displacements in z direction are quite minimal. Consequently, strains and deformations along z axis can be considered negligible. The relationship between stress and strain is established through the stiffness coefficients $\left(\mathrm{Q}_{ij}\right)$ as demonstrated below.

$$\begin{bmatrix} \sigma_x \\ \sigma_y \\ \tau_{yz} \\ \tau_{xz} \\ \tau_{xy} \end{bmatrix} = \begin{bmatrix} \mathrm{Q}_{11} & \mathrm{Q}_{12} & 0 & 0 & 0 \\ \mathrm{Q}_{21} & \mathrm{Q}_{22} & 0 & 0 & 0 \\ 0 & 0 & \mathrm{Q}_{44} & 0 & 0 \\ 0 & 0 & 0 & \mathrm{Q}_{55} & 0 \\ 0 & 0 & 0 & 0 & \mathrm{Q}_{66} \end{bmatrix} \begin{bmatrix} \varepsilon_x \\ \varepsilon_y \\ \gamma_{yz} \\ \gamma_{xz} \\ \gamma_{xy} \end{bmatrix}$$

$$\begin{aligned} Q_{11} &= \tfrac{E(z)}{(1-\nu(z)^2)} \\ Q_{12} &= Q_{11}\,\nu(z) \\ Q_{22} &= Q_{11} \\ Q_{21} &= Q_{12} \\ Q_{44} &= Q_{55} = Q_{66} = \tfrac{E(z)}{2\,(1+\nu(z))} \end{aligned} \tag{6}$$

Below is a detailed description of how forces, moments, and stresses are interrelated.

$$\begin{aligned} \{N_x, N_y, N_{xy}\} &= \int_{-\frac{h}{2}}^{\frac{h}{2}} \{\sigma_x, \sigma_y, \tau_{xy}\}\, dz \\ \{Q_x, Q_y\} &= \int_{-h/2}^{h/2} \{\tau_{xz}, \tau_{yz}\}\, f'(z)\, dz \\ \{M_x^b, M_y^b, M_{xy}^b\} &= \int_{-\frac{h}{2}}^{\frac{h}{2}} \{\sigma_x, \sigma_y, \tau_{xy}\}\, z\, dz \\ \{M_x^s, M_y^s, M_{xy}^s\} &= \int_{-h/2}^{h/2} \{\sigma_x, \sigma_y, \tau_{xy}\}\, f(z)\, dz \end{aligned} \tag{7}$$

By utilizing stress-strain connection defined in Eq. (6) and force-moment-stress interaction outlined in Eq. (7), the corresponding forces and moments for nanoshell are determined.

$$N_x = A_{11}\left(u_{o,x} + \frac{w_0}{R_x}\right) + A_{12}\left(v_{o,y} + \frac{w_0}{R_y}\right) - B_{11}w_{o,xx} - B_{12}w_{o,yy} + A_{s11}\theta_{,x} + A_{s12}\psi_{,y}$$

$$N_y = A_{21}\left(u_{o,x} + \frac{w_0}{R_x}\right) + A_{22}\left(v_{o,y} + \frac{w_0}{R_y}\right) - B_{21}w_{o,xx} - B_{22}w_{o,yy} + A_{s21}\theta_{,x} + A_{s22}\psi_{,y}$$

$$N_{xy} = A_{66}u_{o,y} + A_{66}v_{o,x} - 2B_{66}w_{o,xy} + A_{s66}\theta_{,y} + A_{s66}\psi_{,x}$$

$$Q_x = A_{cc55}\,\theta$$

$$Q_y = A_{cc44}$$

$$M_x^b = B_{11}\left(u_{o,x} + \frac{w_0}{R_x}\right) + B_{12}\left(v_{o,y} + \frac{w_0}{R_y}\right) - D_{11}w_{o,xx} - D_{12}w_{o,yy} + B_{s11}\theta_{,x} + B_{s12}\psi_{,y} \tag{8}$$

$$M_y^b = B_{21}\left(u_{o,x} + \frac{w_0}{R_x}\right) + B_{22}\left(v_{o,y} + \frac{w_0}{R_y}\right) - D_{21}w_{o,xx} - D_{22}w_{o,yy} + B_{s21}\theta_{,x} + B_{s22}\psi_{,y}$$

$$M_{xy}^b = B_{66}u_{o,y} + B_{66}v_{o,x} - 2D_{66}w_{o,xy} + B_{s66}\theta_{,y} + B_{s66}\psi_{,x}$$

$$M_x^s = A_{s11}\left(u_{o,x} + \frac{w_0}{R_x}\right) + A_{s12}\left(v_{o,y} + \frac{w_0}{R_y}\right) - B_{s11}w_{o,xx} - B_{s12}w_{o,yy} + A_{ss11}\theta_{,x} + A_{ss12}\psi_{,y}$$

$$M_y^s = A_{s21}\left(u_{o,x} + \frac{w_0}{R_x}\right) + A_{s22}\left(v_{o,y} + \frac{w_0}{R_y}\right) - B_{s21}w_{o,xx} - B_{s22}w_{o,yy} + A_{ss21}\theta_{,x} + A_{ss22}\psi_{,y}$$

$$M_{xy}^b = A_{s66}u_{o,y} + A_{s66}v_{o,x} - 2B_{s66}w_{o,xy} + A_{ss66}\theta_{,y} + A_{ss66}\psi_{,x}$$

In this context, $A_{ij}, B_{ij}, A_{sij}, D_{ij}, B_{sij}, A_{ccij}$, and A_{ssij} correspond to displacement parameters and are determined according to the calculations provided below.

$$\{A_{ij}, B_{ij}, A_{sij}, D_{ij}, B_{sij}, A_{ccij}, A_{ssij}\} = \int_{-h/2}^{h/2}\{1, z, f(z), z^2, zf(z), f'(z)^2, f(z)^2\}\,Q_{ij}dz \quad i,j = 1,2,6 \tag{9}$$

The equations of motion are formulated through Hamilton's principle, which involves the variations in strain energy caused by the system's deformation, kinetic energy arising from system's motion, and potential energy resulting from external loads applied to system.

$$\delta\int_{t_1}^{t_2}(\Pi - T - V)dt = 0$$

$$\delta\Pi = \int_A\int_{-h/2}^{h/2}\begin{pmatrix}\sigma_x\delta\varepsilon_x + \sigma_y\,\delta\varepsilon_y + \tau_{xy}\delta\gamma_{xy} \\ +\tau_{xz}\delta\gamma_{xz} + \tau_{yz}\delta\gamma_{yz}\end{pmatrix}dz\,dA \tag{10}$$

$$\delta T = \int_A\int_{-h/2}^{h/2}\rho(z)(-\ddot{u}\delta u - \ddot{v}\delta v - \ddot{w}\delta w)\,dz\,dA$$

$$\delta V = \int_A q(x,y)\,\delta w\,dA$$

$$\int_{t_1}^{t_2}\begin{pmatrix}\int_V[\sigma_x\,\delta\varepsilon_x + \sigma_y\delta\varepsilon_y + \tau_{xy}\delta\gamma_{xy} \\ +\tau_{xz}\delta\gamma_{xz} + \tau_{yz}\delta\gamma_{yz} \\ -\rho(z)(-\ddot{u}\delta u - \ddot{v}\delta v - \ddot{w}\delta w)]dv \\ -\int_A[q(x,y)\delta w]dA\end{pmatrix}dt = 0$$

where $\dot{(\,)}$ symbolizes the first time derivative, $\rho(z)$ indicates the mass density, and δ represents the variation.

Eringen's nonlocal elasticity approach offers a comprehensive method for examining nanoscale's impact on nanoshell's the mechanical response. Unlike conventional theories, which assert that stress at a specific point is directly related to the strain at that same location. Eringen's approach proposes that stress at a specific point is influenced by strains throughout the material. This approach reveals how nanoscale characteristics modify the mechanical properties of shell through their stress response. Within the context of Eringen's nonlocal elasticity, the interaction between local and nonlocal stresses is articulated as follows (Eringen, 1972a, b, 1983, Eringen and Edelen 1972):

$$(1 - \mu\,\nabla^2)\sigma_{ij}{}^{nl} = \sigma_{ij}$$
$$\nabla^2 = \partial^2/\partial x^2 + \partial^2/\partial y^2 \tag{11}$$

In this expression, $\sigma_{ij}{}^{nl}$ and σ_{ij} symbolize nonlocal and local stress. Also μ and ∇^2 refer to nonlocal parameter and second order Laplace operator.

The force and moments required for derived motion's equation through Hamilton's principle are expressed in terms of nonlocal stresses, as shown below.

$$\{N_x, N_y, N_{xy}\} = \int_{-\frac{h}{2}}^{\frac{h}{2}}(1 - \mu\,\nabla^2)\{\sigma_x, \sigma_y, \tau_{xy}\}\,dz$$

$$\{Q_x, Q_y\} = \int_{-h/2}^{h/2}(1 - \mu\,\nabla^2)\{\tau_{xz}, \tau_{yz}\}\,f'(z)\,dz$$

$$\{M_x^b, M_y^b, M_{xy}^b\} = \int_{-\frac{h}{2}}^{\frac{h}{2}}(1 - \mu\,\nabla^2)\{\sigma_x, \sigma_y, \tau_{xy}\}\,z\,dz \tag{12}$$

$$\{M_x^s, M_y^s, M_{xy}^s\} = \int_{-h/2}^{h/2}(1 - \mu\,\nabla^2)\{\sigma_x, \sigma_y, \tau_{xy}\}\,f(z)\,dz$$

By incorporating the force and moments from Eq. (12) into Hamilton's principle expressed in Eq. (10), along with displacement and strain components from Eq. (3) and Eq. (5), Hamilton's principle's a more detailed formulation is obtained as follows.

$$\int_{t_1}^{t_2}\begin{pmatrix} -N_{x,x}\delta u_0 + \frac{N_x}{R_x}\delta w_0 - M^b_{x,x,x}\delta w_0 \\ -M^s_{x,x}\delta\theta_0 - N_{y,y}\delta v_0 + \frac{N_y}{R_y}\delta w_0 \\ -M^b_{y,y,y}\delta w_0 - M^s_{y,y}\delta\psi_0 - N_{xy,y}\delta u_0 \\ -N_{xy,y}\delta v_0 - 2M^b_{xy,y,x}\delta w_0 \\ -M^s_{xy,y}\delta\theta_0 - M^s_{xy,x}\delta\psi_0 + Q_x\delta\theta_0 \\ +Q_y\delta\psi_0 + ((1-\mu\nabla^2) \\ (I_1\ddot{u}_0\delta u_0 + 2\frac{I_2\ddot{u}_0}{R_y}\delta u_0 + \frac{I_3\ddot{u}_0}{{R_x}^2}\delta u_0 \\ -I_2\ddot{w}_{0,x}\delta u_0 - \frac{I_3\ddot{w}_{0,x}}{R_x}\delta u_0 + I_4\ddot{\theta}_0\delta u_0 + \\ \frac{I_5\ddot{\theta}_0}{R_x}\delta u_0 + I_1\ddot{u}_0\delta v_0 + 2\frac{I_2\ddot{u}_0}{R_y}\delta v_0 \\ +\frac{I_3\ddot{u}_0}{{R_x}^2}\delta v_0 - I_2\ddot{w}_{0,x}\delta v_0 - \frac{I_3\ddot{w}_{0,x}}{R_x}\delta v_0 + I_4\ddot{\theta}_0\delta v_0 \\ +\frac{I_5\ddot{\theta}_0}{R_x}\delta v_0 + I_2\ddot{u}_{0,x}\delta w_0 + \frac{I_3\ddot{u}_{0,x}}{R_x}\delta w_0 \\ -I_3\ddot{w}_{0,x,x}\delta w_0 + \frac{I_3\ddot{v}_{0,y}}{R_y}\delta w_0 + I_5\ddot{\psi}_{0,y}\delta w_0 \\ +I_5\ddot{\theta}_{0,x}\delta w_0 + I_2\ddot{v}_{0,y}\delta w_0 - I_3\ddot{w}_{0,y,y}\delta w_0 \\ +I_1\ddot{w}_0\delta w_0 + I_4\ddot{u}_0\delta\theta_0 + \frac{I_5\ddot{u}_0}{R_x}\delta\theta_0 \\ -I_5\ddot{w}_{0,x}\delta\theta_0 + I_6\ddot{\theta}_0\delta\theta_0 + I_4\ddot{v}_0\delta\psi_0 \\ +\frac{I_5\ddot{v}_0}{R_y}\delta\psi_0 - I_5\ddot{w}_{0,y}\delta\psi_0 + I_6\ddot{\psi}_0\delta\psi_0 \\ -q(x,y)\delta w_0)) \end{pmatrix} dt = 0 \quad (13)$$

where the inertia components I, are determined utilizing the calculations provided below.

$$\{I_1, I_2, I_3, I_4, I_5, I_6\} = \int_{-h/2}^{h/2}\rho(z)\{1, z, z^2, f(z), zf(z), f(z)^2\}\,dz \quad (14)$$

Eq. (13) is then grouped under δu_0, δv_0, δw_0, $\delta\theta_0$ and $\delta\psi_0$, resulting in the following motion's equations.

$$\begin{gathered} -N_{x,x} - N_{xy,y} + (1-\mu\nabla^2)\left(I_1\ddot{u}_o + 2\,I_2\frac{\ddot{u}_o}{R_x} + I_3\frac{\ddot{u}_o}{{R_x}^2} - I_2\ddot{w}_{o,x} - I_3\frac{\ddot{w}_{o,x}}{R_x} + I_4\ddot{\theta}_0 + I_5\frac{\ddot{\theta}_0}{R_x}\right) = 0 \\ -N_{y,y} - N_{xy,x} + (1-\mu\nabla^2)\left(I_1\ddot{v}_o + 2\,I_2\frac{\ddot{v}_o}{R_y} + I_3\frac{\ddot{v}_o}{{R_y}^2} - I_2\ddot{w}_{o,y} - I_3\frac{\ddot{w}_{o,y}}{R_y} + I_4\ddot{\psi}_0 + I_5\frac{\ddot{\psi}_0}{R_y}\right) = 0 \\ -M^b_{x,xx} - M^b_{y,yy} - 2M^b_{xy,xy} + \frac{N_x}{R_x} + \frac{N_y}{R_y} + (1-\mu\nabla^2)\left(I_1\ddot{w}_o + I_2(\ddot{u}_{o,x} + \ddot{v}_{o,y}) - I_3(\ddot{w}_{o,xx} + \ddot{w}_{o,yy}) + \frac{I_3\ddot{u}_{o,x}}{R_x} + \frac{I_3\ddot{v}_{o,y}}{R_y} + I_5(\ddot{\theta}_{0,x} + \ddot{\psi}_{0,y}) - q(x,y)\right) = 0 \\ -M^s_{x,x} - M^s_{xy,y} + Q_x + (1-\mu\nabla^2)\left(I_4\ddot{u}_o + I_5\frac{\ddot{u}_o}{R_x} - I_5\ddot{w}_{o,x} + I_6\ddot{\theta}_o\right) = 0 \\ -M^s_{y,y} - M^s_{xy,x} + Q_y + (1-\mu\nabla^2)(I_4\ddot{v}_o + I_5\frac{\ddot{v}_o}{R_y} - I_5\ddot{w}_{o,y} + I_6\ddot{\psi}_0) = 0 \end{gathered} \quad (15)$$

The motion equations in Eq. (15) are tackled utilizing an analytical approach known as Navier method, which employs double Fourier series. This technique is particularly efficient for addressing simply behaviour of FG nanoshell with simply supported boundary conditions. By expressing the displacements as Fourier series, Navier method simplifies the resolution process by breaking down complex displacements into basic trigonometric elements. The displacement functions for simply supported FG nanoshell, expressed through Fourier series, are detailed below.

$$\begin{gathered} u_o(x,y,t) = \sum_{m=1}^{\infty}\sum_{n=1}^{\infty} U_{mn}\,Cos\left(\frac{m\pi}{a}x\right)\,Sin\left(\frac{n\pi}{b}y\right)Sin(i\omega t) \\ v_o(x,y,t) = \sum_{m=1}^{\infty}\sum_{n=1}^{\infty} V_{mn}Sin\left(\frac{m\pi}{a}x\right)Cos\left(\frac{n\pi}{b}y\right)Sin(i\omega t) \\ w_o(x,y,t) = \sum_{m=1}^{\infty}\sum_{n=1}^{\infty} W_{mn}\,Sin\left(\frac{m\pi}{a}x\right)\,Sin\left(\frac{n\pi}{b}y\right)Sin(i\omega t) \\ \theta(x,y,t) = \sum_{m=1}^{\infty}\sum_{n=1}^{\infty} \theta_{mn}\,Cos\left(\frac{m\pi}{a}x\right)\,Sin\left(\frac{n\pi}{b}y\right)Sin(i\omega t) \\ \psi(x,y,t) = \sum_{m=1}^{\infty}\sum_{n=1}^{\infty} \psi_{mn}\,Sin\left(\frac{m\pi}{a}x\right)\,Cos\left(\frac{n\pi}{b}y\right)Sin(i\omega t) \end{gathered} \quad (16)$$

In this context, U_{mn}, V_{mn}, W_{mn}, θ_{mn} and ψ_{mn} denote displacement-related variables that are required to satisfy the following boundary conditions for simply supported FG nanoshell.

$$\begin{array}{llll} u_0(x,0,t) = 0 & u_o(x,b,t) = 0 & v_o(0,y,t) = 0 & v_o(a,y,t) = 0 \\ w_o(x,0,t) = 0 & w_o(x,b,t) = 0 & w_o(0,y,t) = 0 & w_o(a,y,t) = 0 \\ M^s_y(x,0,t) = 0 & M^s_y(x,b,t) = 0 & M^s_x(0,y,t) = 0 & M^s_x(a,y,t) = 0 \\ M^b_y(x,0,t) = 0 & M^b_y(x,b,t) = 0 & M^b_x(0,y,t) = 0 & M^b_x(a,y,t) = 0 \\ \theta(x,0,t) = 0 & \theta(x,b,t) = 0 & \psi(0,y,t) = 0 & \psi(a,y,t) = 0 \\ N_y(x,0,t) = 0 & N_y(x,b,t) = 0 & N_x(0,y,t) = 0 & N_x(a,y,t) = 0 \end{array} \quad (17)$$

The vertical distributed dynamic load acting on the system is formulated by employing a double series expansion of trigonometric functions, as detailed below.

$$q(x,y,t) = \sum_{m=1}^{\infty}\sum_{n=1}^{\infty} Q_{mn}(t)\ Sin\left(\frac{m\pi x}{a}\right) Sin\left(\frac{n\pi y}{b}\right)$$
$$Q_{mn}(t) = \frac{4}{ab}\int_{-a/2}^{a/2}\int_{-b/2}^{b/2} q(x,y,t)\, Sin\left(\frac{m\pi x}{a}\right) Sin\left(\frac{n\pi y}{b}\right) dydx \tag{18}$$

Laplace transform provides a means to convert time-variable functions into linear algebraic equations. This approach streamlines equations' solution by removing the necessity of selection an appropriate time step. The following section outlines the procedure for applying Laplace transform to functions that vary with time (Calim and Cuma 2022, 2023, Cuma and Calim 2021a, b, 2022, Türker *et al*. 2023).

$$L[f(t)] = \bar{F}(s) = \int_0^{\infty} f(t)e^{-st} \tag{19}$$

s signifies the variable associated with Laplace transform. The first and second derivatives of $f(t)$, which depend on time, are illustrated in Laplace domain as indicated below. The system is assumed to be in a state of rest at the beginning. Therefore, the initial conditions are set as $f(0) = 0$ and $\dot{f}(0) = 0$.

$$L\left[\dot{f}(t)\right] = s\,\bar{F}(s) - f(0)$$
$$L\left[\ddot{f}(t)\right] = s^2\bar{F}(s) - sf(0) - \dot{f}(0) \tag{20}$$

When the displacements represented by Fourier series in Eq. (16), along with the forces and moments outlined in Eq. (8), are incorporated into the equations of motion and reformulated in matrix notation, the resulting expression is shown below.

$$\left(\begin{bmatrix} k_{11} & k_{12} & k_{13} & k_{14} & k_{15} \\ . & k_{22} & k_{23} & k_{24} & k_{25} \\ . & . & k_{33} & k_{34} & k_{35} \\ . & . & . & k_{44} & k_{45} \\ . & . & . & . & k_{55} \end{bmatrix} + s^2\left(1+\mu(\alpha^2+\beta^2)\right)\begin{bmatrix} m_{11} & m_{12} & m_{13} & m_{14} & m_{15} \\ . & m_{22} & m_{23} & m_{24} & m_{25} \\ . & . & m_{33} & m_{34} & m_{35} \\ . & . & . & m_{44} & m_{45} \\ . & . & . & . & m_{55} \end{bmatrix}\right)$$
$$\begin{bmatrix} \bar{U}_{mn} \\ \bar{V}_{mn} \\ \bar{W}_{mn} \\ \bar{\theta}_{mn} \\ \bar{\psi}_{mn} \end{bmatrix} = \left(1+\mu(\alpha^2+\beta^2)\right)\begin{bmatrix} \bar{P}_x \\ \bar{P}_y \\ \bar{Q}_{mn} \\ \bar{m}_x \\ \bar{m}_y \end{bmatrix} \tag{21}$$

Furthermore, the matrix can be expressed in closed form, as illustrated in the following.

$$\left[\boldsymbol{K}_{mn} + s^2\left(1+\mu(\alpha^2+\beta^2)\right)\boldsymbol{M}_{mn}\right]\bar{\boldsymbol{D}}_{mn} = \left(1+\mu(\alpha^2+\beta^2)\right)\bar{\boldsymbol{F}}_{mn} \tag{22}$$

In this formulation, $\bar{\boldsymbol{D}}_{mn}$ symbolizes the unknown displacement vector, while $\bar{\boldsymbol{F}}_{mn}$ refers to the external force vector in Laplace domain. Additionally, the stiffness and mass matrices are symbolized by $\boldsymbol{K}_{mn}$ and $\boldsymbol{M}_{mn}$. Additionally, the displacements obtained from the matrix solution are in Laplace domain. Durbin's method has been employed to transform these displacements back into time domain. For further details on this transformation, the following references can be consulted (Calim 2003, Temel *et al*. 2004, Calim and Özbey, 2023, Cuma *et al*. 2023, Özbey *et al*. 2024).

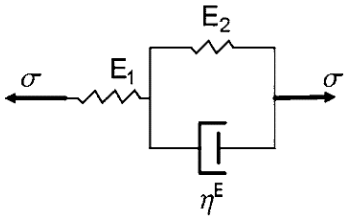

Fig. 2 Linear standard viscoelastic model

Forced vibration analysis can be carried out in either damped or undamped forms. For this purpose, elastic and viscoelastic material models are utilized. While elastic models simplify the solution process, viscoelastic models yield more realistic outcome due to the material's internal friction. By employing the correspondence principle outlined by Boley and Weiner (1960), viscoelastic models can be incorporated into the analysis, allowing elastic constants to be replaced with their viscoelastic counterparts.

A comprehensive literature review has revealed that one of the most widely used viscoelastic models is linear standard viscoelastic model illustrated in Fig. 2. This model facilitates the transition from elastic material properties to viscoelastic material models, as outlined below.

In this framework, $\bar{E}_v$ refers to Young's modulus for viscoelastic materials, and $\bar{G}_v$ corresponds to shear modulus within the same category (Eratlı *et al*. 2014).

$$\bar{E}_v(z) = \bar{E}(z)\left(\frac{1+\beta^G\tau_r^G s}{1+\tau_r^G s}\right)$$
$$\bar{G}_v(z) = \bar{G}(z)\left(\frac{1+\beta^G\tau_r^G s}{1+\tau_r^G s}\right) \tag{23}$$

where β^G illustrates the proportion of the instantaneous value, whereas τ_r^G denotes the retardation time linked to the relaxation function specific to linear standard model and are calculated as indicated below.

$$\tau_r^G = \frac{\eta^E}{E_1+E_2}, \qquad \beta^G = \frac{E_1+E_2}{E_2} > 1 \tag{24}$$

3. Numerical examples

This paper explores the response of simply supported FG porous viscoelastic nanoshell subjected to dynamic distributed loads, analysing how various material and geometric properties affects FG porous viscoelastic nanoshell's behaviour. FG nanoshell's displacement fields

are determined by employing shape function based on HSDT. The governing motion equations are formulated utilizing Hamilton's principle incorporating energy terms and solved analytically via Navier's method. By computing the displacements in Laplace domain, the requirement to select specific time step is bypassed Subsequently, the displacements are reverted to time domain through Durbin's technique's application. Nanoshell's material properties are modelled with linear standard viscoelastic approach to capture realistic material behaviour. In light of this data, a computation method is developed utilizing Mathematica software, and free vibration analysis for FG porous nanoshell is conducted to validate this method's accuracy. The resulting fundamental frequencies are then compared with those reported in existing literature to confirm the model's reliability. Subsequently, within the scope of a parametric study, a series of forced vibration analyses are performed by applying a dynamic distributed load to FG porous viscoelastic nanoshell. Initially, the variation in FG porous viscoelastic nanoshell's displacement-time relationship is examined with respect to different the retardation times linked to the relaxation function, porosity, nonlocal, and power law parameters. Following this, a detailed investigation is carried out on the influences of viscoelastic parameters, including the retardation times linked to the relaxation function and the proportion of the instantaneous value, on FG porous viscoelastic nanoshell's displacement-time relationship. Lastly, a series of maximum displacement analyses are conducted, where FG porous viscoelastic nanoshell's maximum displacements are evaluated. First, the influences of different shell geometries, nonlocal, and power law parameters are examined. Next, the influence of varying nanoshell geometries, porosity distributions, as well as porosity and power law parameters are analysed. Lastly, the study investigates the changes in maximum displacements considering various nanoshell geometries, nanoshell thicknesses, and radii of curvature.

3.1 Validation

In order verify the proposed method's accuracy, free vibration analysis for simply supported FG porous nanoshell is carried out. The variation of FG nanoshell's dimensionless fundamental frequencies is obtained for different shell geometries (spherical shell, cylindrical shell and plate), porosity distributions (even and uneven porosity distributions), and power law $(k = 1, 2)$, nonlocal $(\mu = 0, 1, 2, 4)$ and porosity parameters $(\xi = 0{,}0.3)$. The results are then compared with those of Van Vinh *et al*. (2023), demonstrating the proposed method's accuracy. The analysed FG porous nanoshell's geometric properties can be found in Table 1, while material properties are detailed in Table 2.

The variation dimensionless fundamental frequencies with different shell geometries, porosity distribution, power law, nonlocal and porosity parameter is provided in Table 3. As observed in Table 3, the dimensionless fundamental frequencies obtained are consistent with those in Vinh *et al*. (2023) from literature, confirming proposed method's accuracy.

Table 1 FG porous nanoshell's geometric properties

$h\ (nm)$	$h_0\ (nm)$	$S_0\ (nm^2)$	$R_x\ (nm)$	$a\ (nm)$	$b\ (nm)$
0.5	1	100	20	10	10

Table 2 FG porous nanoshell's material properties

Properties	Metal $(SUS304)$	Ceramic (Al_2O_3)
$E\ (GPa)$	201.02	349.55
$\rho\ (kg/m^3)$	8166	3800
ν	0.3262	0.24

3.2 Parametric Study

A parametric study is conducted by applying a dynamic distributed load on FG porous viscoelastic nanoshell and performing damped forced vibration analysis. FG porous nanoshell's material properties are modelled utilizing linear standard viscoelastic model to obtain more realistic results. For computational convenience, displacements are first obtained in Laplace domain and then transformed back into time domain employing Durbin's method. The magnitude of dynamic distributed load applied to nanoshell is $10^3\ N/m^2$. The total analysis time is set to $2.56 \times 10^{-10}\ s$, with 512 Laplace parameters used. The coefficients m and n are taken as 21 for the iteration. Nanoshell's material properties used in the analysis are applied as provided in Table 2. Nanoshell under analysis has length equal to its width, both set $10\ nm$, with thickness of $0.5\ nm$. Additionally, shell geometry is spherical, with curvature radii in x and y directions taken as $40\ nm$. In this example, the proportion of the instantaneous value (β^G) is taken as constant and set to 1.5. Fig. 3 illustrates how displacement over time for FG porous viscoelastic nanoshell is influenced by changes in the retardation times linked to the relaxation function $(\tau_r^G = static, 0,5 \times 10^{-13}, 1 \times 10^{-12})$ and porosity $(\xi = 0.1, 0.3)$, nonlocal $(\mu = 0{,}1{,}4)$ and power law $(k = 1, 5)$ parameters.

The impact of various the retardation times linked to the relaxation function, as well as the influences of porosity, nonlocal and power law parameters on displacement-time response of FG porous viscoelastic spherical nanoshell subjected to distributed dynamic load of $10^3\ N/m^2$, can be observed in Fig. 3. Power law parameter (k) is set to 0, material consist entirely of ceramic. As this parameter increases, material transitions from ceramic to metal. As noted in Table 2, ceramic's Young's modulus is higher than that of metal, meaning that as power law parameter increases, material strength decreases. Consequently, as expected, Fig. 3 illustrates that an increase in power law parameter leads to higher displacements. An increase in nonlocal parameter (μ) amplifies nanoscale impacts, which in turn enhances shell's fragility and reduces its stiffness. As a results, as depicted in Fig. 3, the rise in nonlocal parameter leads to increase in displacements. Porosity describes presence of voids within material structure. As porosity parameter (ξ) increases, it naturally weakens shell's stiffness. Consistent with expectations, Fig.

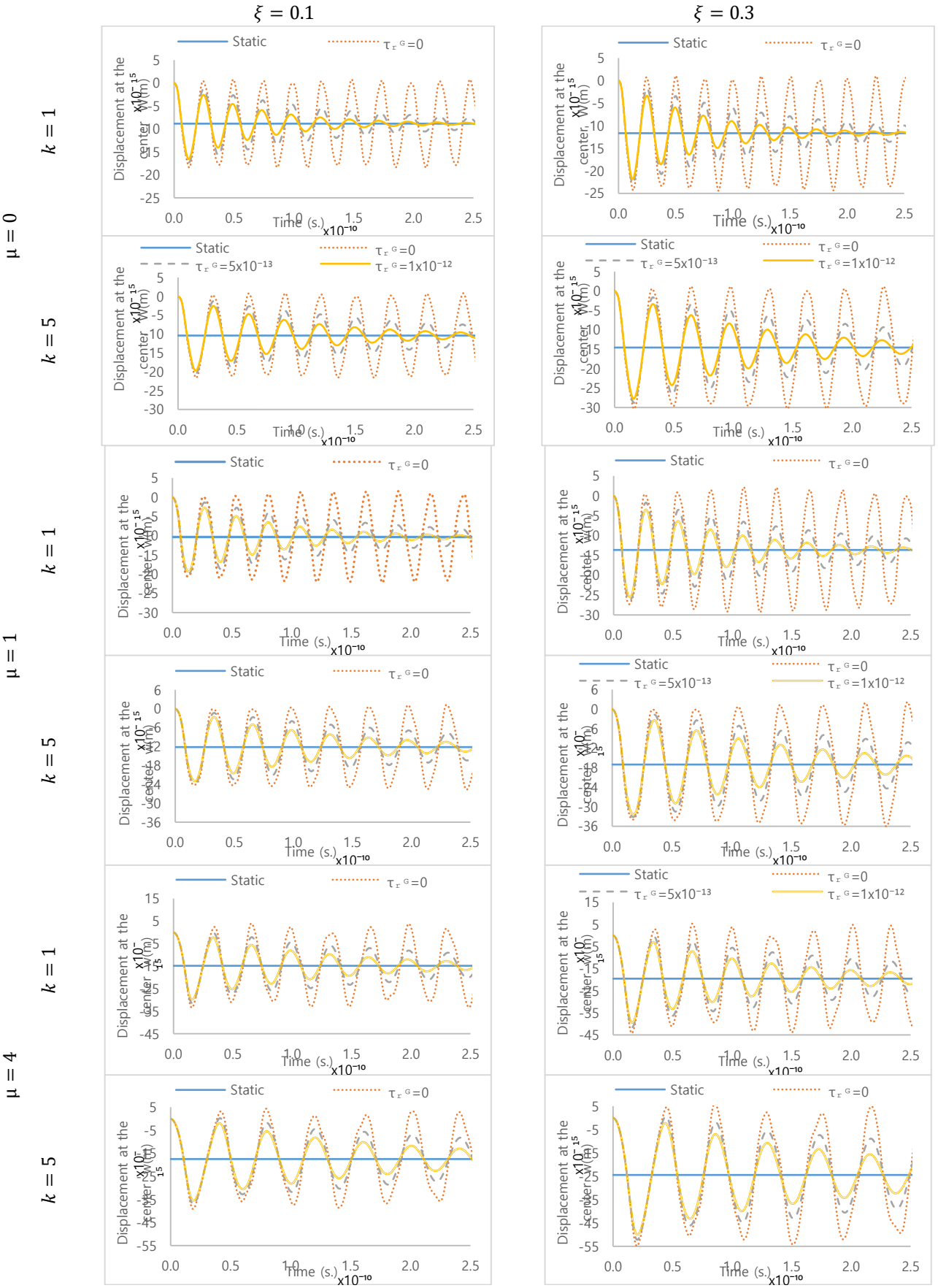

Fig. 3 The variation of temporal displacement behaviour of FG porous viscoelastic nanoshell with the retardation times linked to the relaxation function and porosity, nonlocal, and power law parameters

Table 3 FG porous nanoshell's dimensionless fundamental frequencies $\bar{\omega} = \omega \frac{S_0}{h_0}\sqrt{\frac{\rho_c}{E_c}}$

ξ	μ	Spherical shell $(R_x = R_y)$				Cylindrical shell $(R_y = \infty)$				Plate $(R_x = R_y = \infty)$			
		$k = 1$		$k = 2$		$k = 1$		$k = 2$		$k = 1$		$k = 2$	
		Vinh *et al.* (2023)	Present	Vinh *et al.* (2023)	Present	Vinh *et al.* (2023)	Present	Vinh *et al.* (2023)	Present	Vinh *et al.* (2023)	Present	Vinh *et al.* (2023)	Present
0	0	3.9764	3.9870	3.5961	3.6068	2.6325	2.6497	2.3969	2.4139	2.0590	2.0590	1.8921	1.8918
	1	3.6339	3.6435	3.2864	3.2962	2.4058	2.4215	2.1904	2.2051	1.8817	1.8817	1.7292	1.7288
	2	3.3669	3.3759	3.0449	3.0540	2.2290	2.2436	2.0295	2.0431	1.7435	1.7434	1.6021	1.6018
	4	2.9724	2.9803	2.6882	2.6962	1.9679	1.9807	1.7917	1.8037	1.5392	1.5392	1.4144	1.4142
0.3 Even porosity distribution	0	3.9491	3.9556	3.4179	3.4252	2.5833	2.5988	2.2538	2.2678	1.9896	1.9896	1.7562	1.7558
	1	3.6089	3.6149	3.1235	3.1302	2.3608	2.3749	2.0597	2.0724	1.8182	1.8182	1.6050	1.6046
	2	3.3438	3.3493	2.8940	2.9002	2.1874	2.2005	1.9084	1.9202	1.6847	1.6847	1.4871	1.4867
	4	2.9521	2.9569	2.5549	2.5604	1.9311	1.9427	1.6848	1.6952	1.4873	1.4873	1.3128	1.3125
0.3 Uneven porosity distribution	0	4.0149	4.0248	3.5702	3.5804	2.6861	2.7034	2.4094	2.4252	2.1274	2.1268	1.9297	1.9284
	1	3.6690	3.6781	3.2627	3.2720	2.4548	2.4706	2.2019	2.2163	1.9442	1.9436	1.7634	1.7623
	2	3.3995	3.4079	3.0230	3.0317	2.2744	2.8909	2.0401	2.0535	1.8013	1.8008	1.6339	1.6328
	4	3.0012	3.0086	2.6688	2.6765	2.0080	2.0209	1.8011	1.8129	1.5903	1.5898	1.4425	1.4415

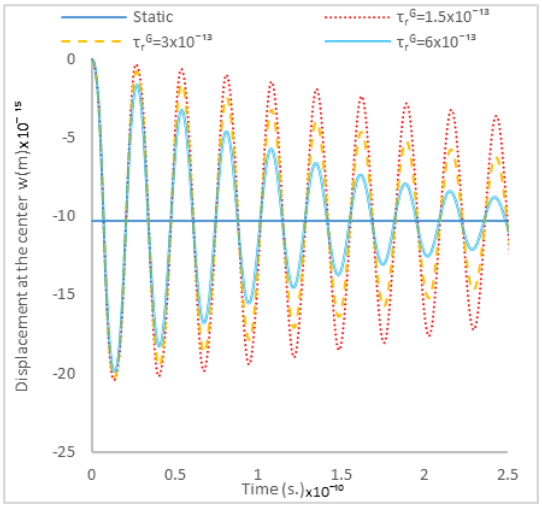

$\beta^G = 1.5$

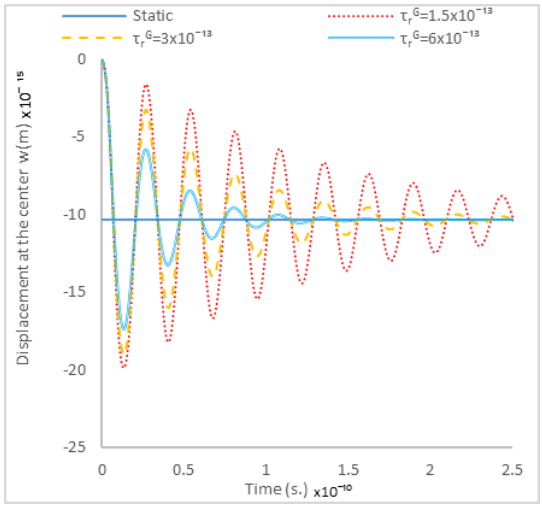

$\beta^G = 3$

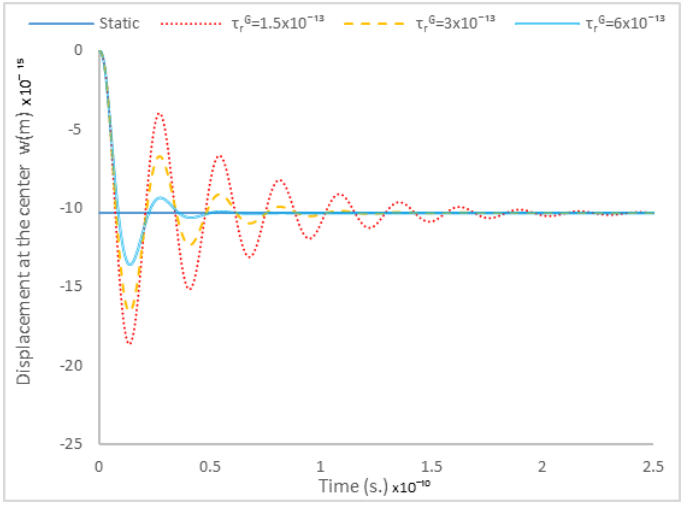

$\beta^G = 6$

Fig. 4 The variation of temporal displacement behaviour of FG porous viscoelastic nanoshell with the retardation times linked to the relaxation function and the proportion of the instantaneous value

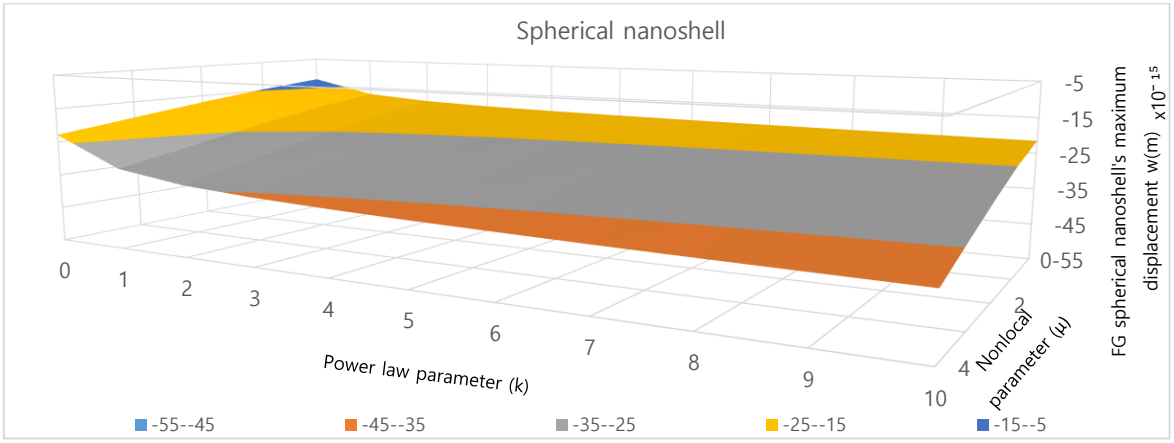

(a)

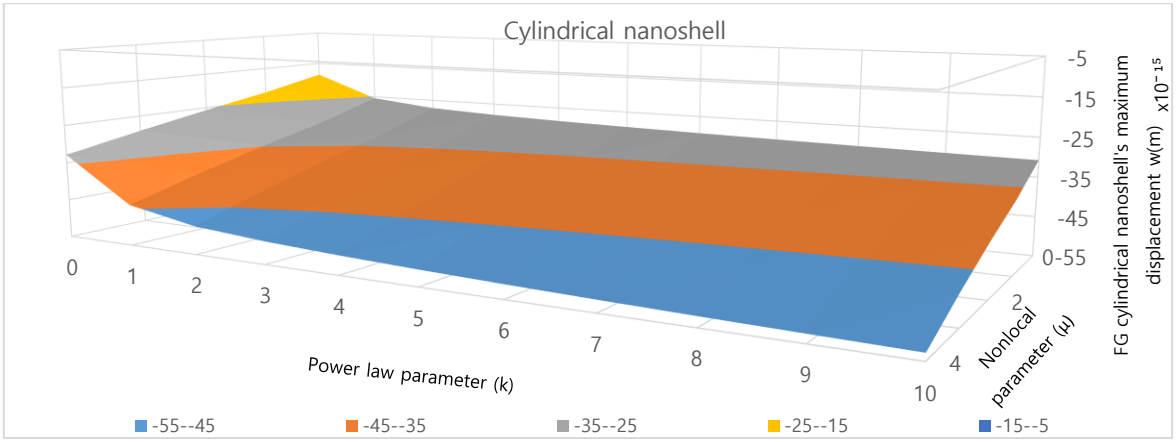

(b)

Fig. 5 The variation of maximum displacement behaviour of FG porous viscoelastic nanoshell with shell geometries, nonlocal and power law parameters

3 demonstrates that higher porosity levels result in greater displacements. It is also observed that the retardation times linked to the relaxation function (τ_r^G) gradually decrease displacements, causing them to stabilize at constant value over time. Furthermore, an increase in τ_r^G accelerates this reduction, leading to a quicker stabilization. Additionally, when examining nonlocal parameter's influence on damping within analysis, it is observed that an increment in this parameter reduces damping's impact on displacements. Examining the impact of power law parameter alongside nanoscale influence and porosity reveals that increases in both porosity and nonlocal parameters amplify power law parameter's influence. This occurs because, similar to power law parameter, increases in porosity and nonlocal parameters lead to a reduction in nanoshell's stiffness. The same applies to porosity parameter's impact on displacements in relation to the other two parameters, as well as nonlocal parameter's influence on displacements in relation to the other two parameters. Additionally, when examining periods in Fig. 3, the following conclusions are drawn: an increase in power law parameter leads to longer periods. Moreover, it is observed that the retardation times linked to the relaxation function do not have a significant effect on periods. When nonlocal parameter is 1, periods are smaller compared to when it is 5. Similar to the other two parameters, an increase in porosity parameter results in longer periods. Additionally, the largest displacement and periods occur when nonlocal, porosity, and power law parameters are all at their maximum values. Finally, it can be stated that the increase in nonlocal and power law parameters reduces the damping effect. It is observed that at lower values of both parameters, displacements tend to dampen more rapidly.

In addition to this study, a detailed investigation is carried out on FG porous viscoelastic spherical nanoshell's displacement-time relationship, considering linear standard viscoelastic material coefficients, including the retardation time linked to the relaxation function ($\tau_r^G = Static, 1.5 \times 10^{-13}, 3 \times 10^{-13}, 6 \times 10^{-13}$) and the proportion of the instantaneous value($\beta^G = 1.5, 3, 6$). The analysis uses the same material and geometric properties, total solution time, radius of curvature, and uniformly distributed dynamic load as the previous example. Additionally, porosity, nonlocal, and power law parameters are kept constant at 0.1, 1 and 1, respectively.

In Fig. 4, the influence of various values of the retardation time linked to the relaxation function and the proportion of the instantaneous value on FG porous viscoelastic spherical nanoshell's displacement-time response is analysed. In the study by Calim and Özbey (2023), FG

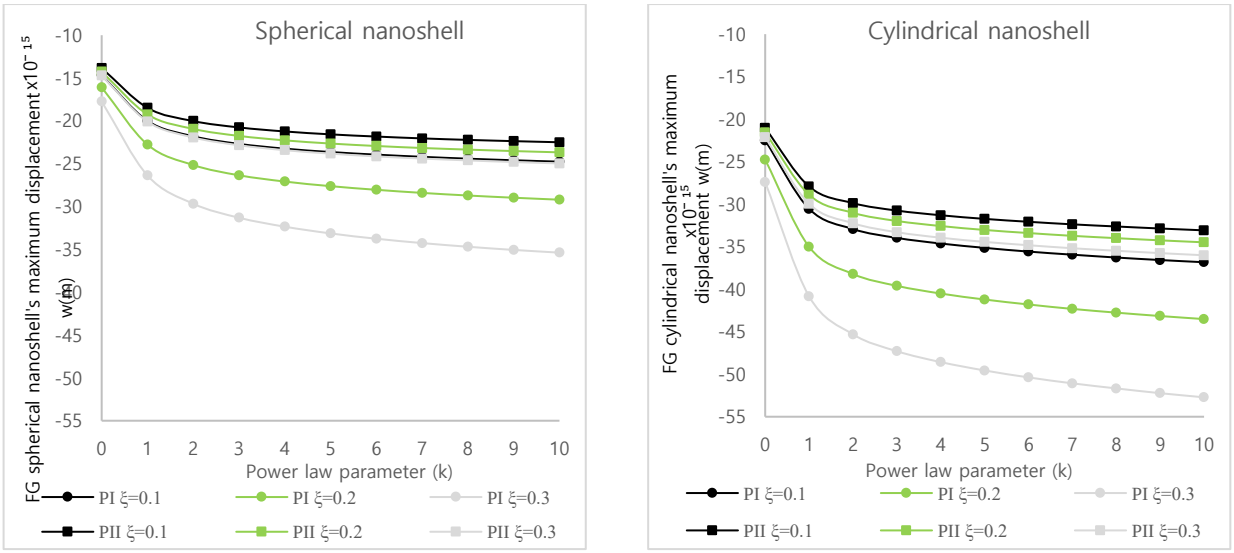

(a) (b)

Fig. 6 The variation of maximum displacement behaviour of FG porous viscoelastic nanoshell with porosity distribution, shell geometries and porosity and power law parameters

porous viscoelastic shell's displacement-time relationship was investigated. They used β^G values of $1.1, 2, 3, 4$ and τ_r^G values of $2\times10^{-5}, 4\times10^{-5}, 10\times10^{-5}$ to achieve a stable oscillation and damping. In the current study, β^G values of 1.5, 3, 6 and τ_r^G values of $1.5\times10^{-13}, 3\times10^{-13}$, 6×10^{-13} are employed. From this, it can be deduced that nanoscale influences have no significant impact on β^G. However, the substantial difference between τ_r^G values used in both studies highlights the clear influence of nanoscale effects on τ_r^G. τ_r^G reduces displacements over time, stabilizing them at a constant value. Moreover, as τ_r^G increases, it not only accelerates this reduction but also decreases displacements to a greater extent. It is also observed that an increase in β^G amplifies τ_r^G's impact on the analysis. Similar to τ_r^G, β^G promotes a gradual reduction and further decreasing displacements. Additionally, an increase in β^G enhances τ_r^G's impact on the analysis. Neither of these parameters shows a significant influence on the periods. Furthermore, analyses are performed for double increments of both parameters. It is evident that when τ_r^G and β^G are increased at the same rate, the effect of increasing β^G on the analysis is more pronounced than that of τ_r^G.

As part of parametric analysis, maximum displacements of FG porous viscoelastic nanoshell are evaluated with respect to varying shell geometries and different values of nonlocal and power law parameters. For this purpose, a dynamic distributed load of $10^3\,N/m^2$ is applied to nanoshell. The total analysis time, the proportion of the instantaneous value, the retardation time linked to the relaxation function, and porosity parameter are kept constant at $2.56\times10^{-10}\,s, 1.5, 5\times10^{-13}$, and 0.1, respectively. Fig. 5(a) presents maximum displacements' variation for spherical nanoshell in relation to nonlocal and power law parameters, while Fig. 5(b) illustrates the same for a cylindrical nanoshell. For spherical shell, the radii of curvature in both x and y directions are equal at 40 nm, while for cylindrical shell, they are set at 40 nm and infinity, respectively. Additionally, the values of m and n are set to 21 for iteration. Also, the geometric and material properties of nanoshell in current analysis are assumed to be identical to those in the previous example.

Fig. 5(a) presents the variation of maximum displacements in spherical nanoshell both in relation to nonlocal and power law parameters, while Fig. 5(b) shows the same for cylindrical shells. For both shell geometries, it is observed that as nonlocal parameter increases, the displacements also increase, which can be attributed to the rise in FG nanoshell's flexibility. The increase in nonlocal parameter results in a similar rate of displacement increase across all values of power law parameter. Additionally, the rate of increase in displacement due to the nonlocal parameter is more pronounced in cylindrical nanoshells than in spherical nanoshells. The increase in the power law parameter, which leads to a reduction in Young's modulus, also causes an increase in displacements. This increase is more significant at lower values of the power law parameter, and as the parameter increases, the rate of change in displacements decreases. Notably, a sharp change in displacements between power law values of 0 and 1 is evident for both shell geometries. Furthermore, Fig. 5 clearly shows that displacements in cylindrical shells are larger than those in spherical shells. This can be explained by the increase in the radius of curvature, which enhances nanoshell's flexibility, and the fact that the cylindrical shells have an infinite radius of curvature in the y-direction.

In the continuation of parametric study, the maximum displacements of FG nanoshell under dynamic distributed load of $10^3\,N/m^2$ are analysed, considering various shell geometries (spherical and cylindrical shells), power law parameters $(k = 1-10)$, porosity distributions (even (PI) and uneven (PII) porosity distribution), and porosity parameters $(\xi = 0.1, 0.2, 0.3)$. The same material properties as in the previous example are used in the analysis. The

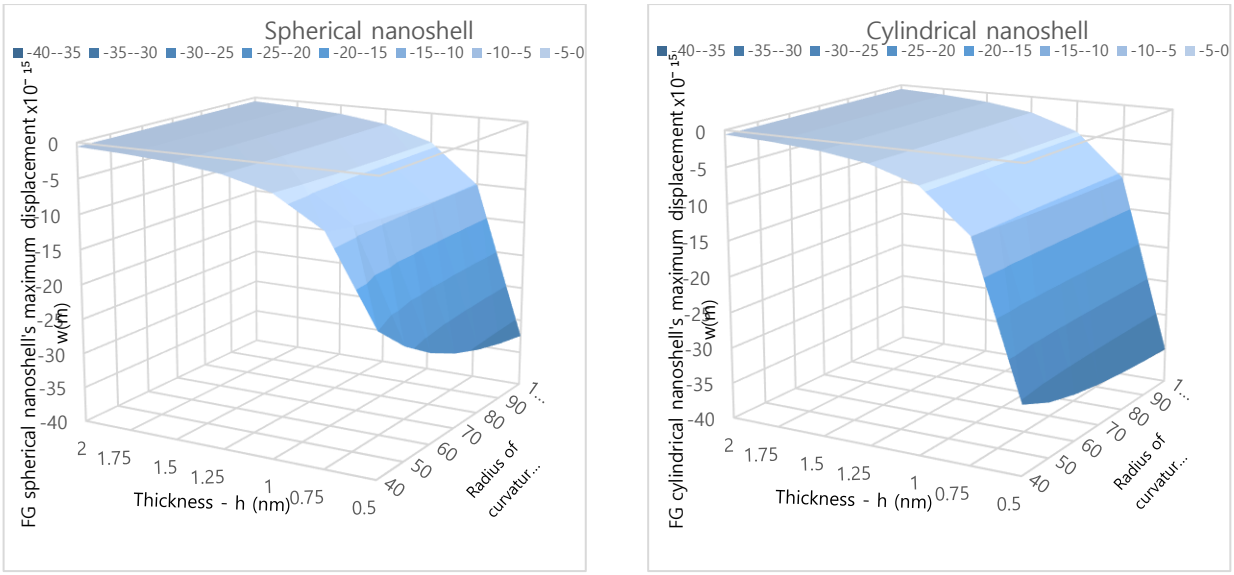

(a) (b)

Fig. 7 The variation of maximum displacement behaviour of FG porous viscoelastic nanoshell with shell geometries radii of curvature and thicknesses

examined nanoshell's geometrical dimensions are $a = b = 10\,nm$ and $h = 0.5\,nm$. The radii of curvature are $R_x = 40\,nm$ and $R_y = \infty$ for cylindrical nanoshell, while the radii of curvature are $R_x = R_y = 40\,nm$ for spherical nanoshell. Additionally, the parameters $\beta^G = 1.5$, $\tau_r^G = 5 \times 10^{-13}$, and $\mu = 1$ are employed in the analysis. The total solution time is set to $2.56 \times 10^{-10}\,s$ and m and n coefficients are taken as 21 to perform the iteration.

Fig. 6 illustrates the variation in FG nanoshell's maximum displacements based on different porosity parameters and distributions, power law parameters, and shell geometries. As power law parameter increases, the material transitions more rapidly from ceramic to metal, reducing FG porous nanoshell's rigidity. Consequently, as seen in Fig. 6, an increase in power law parameters leads to an increment in FG porous nanoshell's displacements, with this effect being more pronounced at lower values of power law parameter. The displacement increase is most significant between power law values of 0 and 1, while for larger values, the increment in displacement diminishes and tends to stabilize. Additionally, the increment in displacements caused by power law parameter is more pronounced at higher porosity parameters. Furthermore, the influence of power law parameter on displacements is similar for both porosity distributions, with the impact being more pronounced in even porosity distribution compared to uneven distribution. As porosity parameter increases, voids-pores within material increase, leading to reduction in nanoshell's stiffness and resulting in larger displacements. This increment becomes more pronounced at higher porosity parameters. Moreover, displacement increase due to the rise in porosity parameter is much more significant for even porosity distribution compared to uneven porosity distribution. Fig. 6 shows that displacements in cylindrical nanoshells are larger than those in spherical nanoshells, which can be attributed to the increased nanoshell's slenderness caused by curvature radius. As power law parameter increases, the curves tend to diverge, but beyond a certain value of power law parameter, the rate of increase in the difference between the curves diminishes. In other words, with an increase in power law parameter, the difference in displacement calculated for different porosity parameters at the same power law parameter grows up to a specific point, after which this growth rate begins to decrease. Lastly, it is clearly observed that the displacements for even porosity distribution are higher than those for uneven porosity distribution. This indicates that pores' even distribution within FG nanoshell leads to a greater reduction in its stiffness. It is also observed that the difference in displacements calculated for various porosity parameters is minimal in uneven porosity distribution, whereas this difference becomes much more pronounced in even porosity distribution.

In the final part of parametric study, the variation of maximum displacements with respect to geometric parameters such as different shell geometries, curvature radii, and nanoshell thickness is examined. A dynamic distributed load of $10^3\,N/m^2$ is applied to nanoshell's surface to calculate maximum displacements. The total analysis time is set to $2.56 \times 10^{-10}\,s$, and 512 Laplace parameters are used. Material properties are taken as provided in Table 2. The width and length of nanoshell are considered to be $10\,nm$. Additionally, power law, nonlocal, and porosity parameters, as well as β^G, and τ_r^G, are held constant at 1, 1, 0.1, 1.5, and 5×10^{-13}, respectively, throughout the analysis. m and n parameters are set to21 to initiate the loop.

Fig. 7(a) presents the variation of maximum displacements for spherical nanoshell, while Fig. 7(b) illustrates the same for cylindrical nanoshell, both plotted against different nanoshell thicknesses and radii of curvature. An increment in the radius of curvature leads to a

rise in displacements, which can be attributed to the increase in nanoshell's slenderness. This impact is more pronounced at smaller values of the radius of curvature. The impact of changes in the radius of curvature on the maximum displacements is more significant in spherical nanoshells compared to cylindrical nanoshells. This is due to the fact the radius of curvature in y direction is taken as infinite and constant for cylindrical nanoshells. Moreover, it is observed that changes in the radius of curvature have a sharp effect on maximum displacements when nanoshell's thickness is smaller. As nanoshell's thickness increases, this effect diminishes considerably. Specifically, for thickness values of 1.5 nm and beyond, the influence of the radius of curvature on maximum displacements becomes significantly reduced. An increment in nanoshell's thickness leads to a reduction in displacements, because nanoshell's slenderness decreases and its rigidity increases. This reduction is more pronounced at lower thickness values. Additionally, an increment in the radius of curvature enhances the impact of thickness on the maximum displacements. It is also observed that the effect of curvature radius variation on the influence of thickness changes on maximum displacements is less significant than the effect of thickness variation on the influence of curvature radius changes on maximum displacements. Moreover, the influence of thickness variation is more prominent in cylindrical nanoshells compared to spherical nanoshells, with higher displacements observed in cylindrical nanoshells. This can be attributed to the increased slenderness caused by the curvature radius and the fact that the radius of curvature in y direction is infinite for cylindrical nanoshells.

4. Conclusions

In this study, the dynamic response of simply supported FG porous viscoelastic nanoshell under step-type uniformly distributed dynamic load is investigated for different geometries. FG porous shell's displacements are obtained utilizing stress and strain shape function based on higher order shear deformation theory. Utilizing HSDT and Eringen's nonlocal elasticity theory, the motion's equations are formulated via Hamilton's principle and solved utilizing Navier method and Laplace domain approach. A computational model developed in Mathematica is validated through free vibration analysis. Parametric studies examine the impacts of viscoelastic coefficients, porosity, non-locality, power law parameters, and nanoshell geometry on displacements. The findings from these analyses are summarized below.

• When power law parameter is zero, the material is fully ceramic. As this parameter increases, the transition to metal accelerates, leading to reduced stiffness and increased displacement and period. This effect is more pronounced at lower power law parameters and this impact tends to stabilize as the parameter increases. Additionally, the displacement increase associated with power law parameter is more pronounced in even porosity distributions compared to uneven porosity distributions.

• A higher nonlocal parameter amplifies nanoscale impacts, decreasing stiffness and increasing displacement and period. This impact is more noticeable in spherical nanoshells at lower values but becomes dominant in cylindrical nanoshells at higher values. Additionally, damping decreases with increasing nonlocal parameter.

• Increasing porosity reduces the material's stiffness, leading to greater displacements and longer periods. The displacement increase is more pronounced in uniform porosity distributions compared to other distributions and is more significant in cylindrical nanoshells than in spherical ones.

• It is observed that porosity, nonlocal, and power law parameters enhance each other's impacts in the analysis. The increasing nonlocal and power law parameters results in a decrease in damping. At lower values of these parameters, the displacements diminish at a faster rate.

• Retardation times associated with the relaxation function and the proportion of the instantaneous value reduce displacements, stabilizing them over time. An increase in these parameters accelerates this reduction, while their impact on periods remains negligible.

• β^G and τ_r^G mutually enhance their impacts on the analysis. While nanoscale impacts have a negligible impact on β^G, their influence on τ_r^G is quite significant. When both β^G and τ_r^G are increased at the same rate, it is evident that the impact of increasing β^G on the analysis is more pronounced than that of τ_r^G.

• A higher curvature radius increases nanoshell's slenderness, resulting in greater displacements. This effect is more pronounced at smaller curvature radius values. Additionally, due to variations in both x and y directions, its influence on displacements is more significant in spherical nanoshells. As thickness increases, this effect diminishes.

• The reduction in nanoshell's thickness increases its fragility and decreases its rigidity, leading to an increase in displacements. An increment in the radius of curvature amplifies impact of nanoshell's thickness on displacements. Thickness variation's impact is more pronounced in cylindrical nanoshells compared to spherical nanoshells.

References

Addou, F.Y., Bourada, F., Tounsi, A., Bousahla, A.A., Tounsi, A., Benrahou, K.H. and Albalawi, H. (2024), "Effect of porosity distribution on flexural and free vibrational behaviors of laminated composite shell using a novel sinusoidal HSDT", *Arch. Civil Mech. Eng.*, **24**(2), 102. https://doi.org/10.1007/s43452-024-00894-w

Alam, M., Guo, Y., Bai, Y. and Luo, S. (2025), "Post-critical nonlinear vibration of nonlocal strain gradient beam involving surface energy effects", *JSV*, **601**, 118930. https://doi.org/10.1016/j.jsv.2025.118930

Alnujaie, A., Daikh, A.A., Ghazwani, M.H., Assie, A.E. and Eltaher, M.A. (2024), "Size-dependent free vibration of coated functionally graded graphene reinforced nanoplates rested on viscoelastic medium", *Adv. Nano Res.*, **17**(2), 181. https://doi.org/10.12989/anr.2024.17.2.181

Altenbach, H. and Eremeyev, V.A. (2011), "On the shell theory on the nanoscale with surface stresses", *Int. J. Eng. Sci.*, **49**(12), 1294-1301. https://doi.org/10.1016/j.ijengsci.2011.03.011

Arefi, M. (2020), "Electro-mechanical vibration characteristics of piezoelectric nano shells", *Thin Wall. Struct.*, **155**, 106912. https://doi.org/10.1016/j.tws.2020.106912

Babagi, P.N., Neya, B.N. and Ghadi, M.E. (2025), "Free vibration and buckling analysis of simply supported rectangular nano-plates: A closed-form solution based on nonlocal 3D elasticity theory", *Int. J. Solids Struct.*, **312**, 113261. https://doi.org/10.1016/j.ijsolstr.2025.113261

Boley, B.A. and Weiner, J.H. (1960), *Theory of Thermal Stresses*, John Wiley and Sons, Ltd.

Calim, F.F. (2003), "Dynamic analysis of viscoelastic, anisotropic curved spatial rod systems", Ph.D. Dissertation, *Cukurova University*, Adana, Turkey (In Turkish).

Calim, F.F. and Cuma, Y.C. (2022), "Vibration analysis of nonuniform hyperboloidal and barrel helices made of functionally graded material", *Mech. Based Des. Struct.*, **50**(11), 3781-3795. https://doi.org/10.1080/15397734.2020.1822181

Calim, F.F. and Cuma, Y.C. (2023), "Forced vibration analysis of viscoelastic helical rods with varying cross-section and functionally graded material", *Mech Based Des. Struct.*, **51**(7), 3620-3631. https://doi.org/10.1080/15397734.2021.1931307

Calim, F.F. and Özbey, M.B. (2023), "Damped response of porous functionally graded viscoelastic cylindrical shells", *Mech. Based Des. Struct.*, 1-20. https://doi.org/10.1080/15397734.2023.2242482

Cao, Y., Khorami, M., Baharom, S., Assilzadeh, H. and Hassan Dindarloo, M. (2021), "The effects of multi-directional functionally graded materials on the natural frequency of the doubly-curved nanoshells", *Compos. Struct.*, **258**, 113403. https://doi.org/10.1016/j.compstruct.2020.113403

Civalek, Ö., Uzun, B. and Yaylı, M.Ö. (2023), "On nonlinear stability analysis of saturated embedded porous nanobeams", *Int. J. Eng. Sci*, **190**, 103898. https://doi.org/10.1016/j.ijengsci.2023.103898

Cong, P.H., Huong, N. Van, Thien, T.T. and Duc, N.D. (2024), "Nonlocal strain gradient-based geometrically nonlinear vibration analysis of double curved shallow nanoshell containing functionally graded layers", *Aerosp. Sci. Technol.*, **151**, 109310. https://doi.org/10.1016/j.ast.2024.109310

Cuma, Y.C. and Calim, F.F. (2021a), "Free vibration analysis of functionally graded cylindrical helices with variable cross-section", *J. Sound and Vib.*, **494**, 115856. https://doi.org/10.1016/j.jsv.2020.115856

Cuma, Y.C. and Calim, F.F. (2021b), "Transient response of functionally graded non-uniform cylindrical helical rods" *Steel Compos. Struct.*, **40**(4), 571-580. https://doi.org/10.12989/scs.2021.40.4.571

Cuma, Y.C. and Calim, F.F. (2022), "Dynamic response of viscoelastic functionally graded barrel and hyperboloidal coil springs with variable cross-sectional area" *Mech. Time Depend. Mater.*, **26**(4), 923-937. https://doi.org/10.1007/s11043-021-09520-1

Cuma, Y.C., Özbey, M.B. and Calim, F.F. (2023), "Vibration and damping analysis of functionally graded shells", *Mech. Time Depend. Mater.*, **28**(4), 2241-2264. https://doi.org/10.1007/s11043-023-09621-z

Dai, H. and Safarpour, H. (2021), "Frequency and thermal buckling information of laminated composite doubly curved open nanoshell", *Adv. Nano Res.*, **10**(1), 1-14. https://doi.org/10.12989/anr.2021.10.1.001

Doan, D.V., Luat, D.T., Avcar, M. and Vinh, P.V. (2025), "Damped vibration characteristics of functionally graded graphene oxide powder-reinforced composite plates using a novel viscoelastic foundation model", *Physica B*, **700**, 416903. https://doi.org/10.1016/j.physb.2025.416903

Eltaher, M.A., Daikh, A.A., Hamdi, A., Abdelhaffez, G.S. and Abdraboh, A.M. (2024a), "Refined nonlocal strain gradient theory for mechanical response of cosine FG-GRNC laminated nanoshells rested on elastic foundation", *Adv. Nano Res.*, **17**(4), 335. https://doi.org/10.12989/anr.2024.17.4.335

Eltaher, M.A., Esen, I., Abdelrahman, A.A. and Abdraboh, A.M. (2024b), "Dynamic response of FG carbon nanotubes nano-plates embedded in elastic media under moving point load", *Adv. Nano Res.*, **17**(3), 257-274. https://doi.org/10.12989/anr.2024.17.3.257

Eratlı, N., Argeso, H., Calim, F.F., Temel, B. and Omurtag, M.H. (2014), "Dynamic analysis of linear viscoelastic cylindrical and conical helicoidal rods using the mixed FEM", *J. Sound Vib.*, **333**(16), 3671-3690. https://doi.org/10.1016/j.jsv.2014.03.017

Eringen, A.C. (1972a), "Linear theory of nonlocal elasticity and dispersion of plane waves", *Int. J. Eng. Sci.*, **10**(5), 425-435. https://doi.org/10.1016/0020-7225(72)90050-X

Eringen, A.C. (1972b), "Nonlocal polar elastic continua", *Int. J. Eng. Sci.*, **10**(1), 1-16. https://doi.org/10.1016/0020-7225(72)90070-5

Eringen, A.C. (1983), "On differential equations of nonlocal elasticity and solutions of screw dislocation and surface waves", *J. Appl. Phys.*, **54**(9), 4703-4710. https://doi.org/10.1063/1.332803

Eringen, A.C. and Edelen, D.G.B. (1972), "On nonlocal elasticity", *Int. J. Eng. Sci*, **10**(3), 233-248. https://doi.org/10.1016/0020-7225(72)90039-0

Eyvazian, A., Shahsavari, D. and Karami, B. (2020), "On the dynamic of graphene reinforced nanocomposite cylindrical shells subjected to a moving harmonic load", *Int. J. Eng. Sci*, **154**, 103339. https://doi.org/10.1016/j.ijengsci.2020.103339

Faleh, N.M., Ahmed, R.A. and Fenjan, R.M. (2018), "On vibrations of porous FG nanoshells", *Int. J. Eng. Sci*, **133**, 1-14. https://doi.org/10.1016/j.ijengsci.2018.08.007

Fang, K., Huang, G., Yu, G., Xu, W. and Yuan, W. (2024), "Free vibration analysis of graphene origami-reinforced nano cylindrical shell", *Mech. Adv. Mat. Struct.*, 1-13. https://doi.org/10.1080/15376494.2024.2315602

Farajpour, A., Ghayesh, M.H. and Farokhi, H. (2018), "A review on the mechanics of nanostructures" *Int. J. Eng. Sci.*, **133**, 231-263. https://doi.org/10.1016/j.ijengsci.2018.09.006

Ghadiri, M. and Safarpour, H. (2016), "Free vibration analysis of embedded magneto-electro-thermo-elastic cylindrical nanoshell based on the modified couple stress theory", *Appl. Phys A.*, **122**(9), 833. https://doi.org/10.1007/s00339-016-0365-4

Ghayesh, M.H. and Farajpour, A. (2019), "A review on the mechanics of functionally graded nanoscale and microscale structures", *Int. J. Eng. Sci*, **137**, 8-36. https://doi.org/10.1016/j.ijengsci.2018.12.001

Ghazwani, M.H., Alnujaie, A., Vinh, P.V. and Civalek, Ö. (2024a), "High frequency analysis of the functionally graded sandwich nanobeams embedded in elastic foundations using nonlocal quasi-3D theory", *Physica B*, **675**, 415646. https://doi.org/10.1016/j.physb.2023.415646

Ghazwani, M.H., Alnujaie, A., Vinh, P.V. and Tounsi, A. (2024b), "A quasi-3D nonlocal theory for free vibration analysis of functionally graded sandwich nanobeams on elastic foundations", *Adv. Nano Res.*, **16**(3), 313-324. https://doi.org/10.12989/anr.2024.15.3.313

He, D., Xu, H., Wang, Y., Wang, M., Duan, Z., Yang, N. and Wang, T. (2025), "Research on vertical vibration characteristics of rolling mill based on magnetorheological fluid damper absorber", *MSSP*, **224**, 112203. https://doi.org/10.1016/j.ymssp.2024.112203

Kachapi, S.H.H. (2020), "Nonlinear and nonclassical vibration analysis of double walled piezoelectric cylindrical nanoshell", *Adv. Nano Res.*, **9**(4), 277-294. https://doi.org/10.12989/anr.2020.9.4.277

Karami, B. and Janghorban, M. (2020), "On the mechanics of functionally graded nanoshells", *Int. J. Eng. Sci*, **153**, 103309. https://doi.org/10.1016/j.ijengsci.2020.103309

Karami, B., Shahsavari, D. and Janghorban, M. (2019), "On the

dynamics of porous doubly-curved nanoshells", *Int. J. Eng. Sci*, **143**, 39-55. https://doi.org/10.1016/j.ijengsci.2019.06.014

Kiani, Y., Akbarzadeh, A.H., Chen, Z.T. and Eslami, M.R. (2012a), "Static and dynamic analysis of an FGM doubly curved panel resting on the Pasternak-type elastic foundation", *Compos. Struct.*, **94**(8), 2474-2484. https://doi.org/10.1016/j.compstruct.2012.02.028

Kiani, Y., Shakeri, M. and Eslami, M. (2012b), "Thermoelastic free vibration and dynamic behaviour of an FGM doubly curved panel via the analytical hybrid Laplace-Fourier transformation", *Acta Mech.*, **223**(6), 1199-1218. https://doi.org/10.1007/s00707-012-0629-9

Mehralian, F., Tadi Beni, Y. and Ansari, R. (2016), "Size dependent buckling analysis of functionally graded piezoelectric cylindrical nanoshell", *Compos. Struct.*, **152**, 45-61. https://doi.org/10.1016/j.compstruct.2016.05.024

Mirjavadi, S.S., Forsat, M., Nia, A.F., Badnava, S. and Hamouda, A.M.S. (2020), "Nonlocal strain gradient effects on forced vibrations of porous FG cylindrical nanoshells", *Adv. Nano Res.*, **8**(2), 149-156. https://doi.org/10.12989/anr.2020.8.2.149

Monge, J.C., Mantari, J.L., Llosa, M.N. and Hinostroza, M.A. (2023), "A size-dependent 3D solution of functionally graded shallow nanoshells", **10**(1). https://doi.org/doi:10.1515/cls-2022-0215

Özbey, M.B. and Calim, F.F. (2025), "Dynamic analysis of viscoelastic functionally graded nanoplate", *Mech. Based Des. Struct.*, 1-25. https://doi.org/10.1080/15397734.2024.2449481

Özbey, M.B., Cuma, Y.C., Deneme, I.O. and Calim, F.F. (2024), "Free and forced vibration analysis of FG-CNTRC viscoelastic plate using high shear deformation theory", *Adv. Nano Res.*, **16**(4), 413-426. https://doi.org/10.12989/anr.2024.16.4.413

Rachid, A., Ouinas, D., Lousdad, A., Zaoui, F.Z., Achour, B., Gasmi, H., Butt, T.A. and Tounsi, A. (2022), "Mechanical behavior and free vibration analysis of FG doubly curved shells on elastic foundation via a new modified displacements field model of 2D and quasi-3D HSDTs", *Thin Wall. Struct.*, **172**, 108783. https://doi.org/10.1016/j.tws.2021.108783

Rouhi, H., Ansari, R. and Darvizeh, M. (2016), "Size-dependent free vibration analysis of nanoshells based on the surface stress elasticity", *Appl. Math. Model.*, **40**(4), 3128-3140. https://doi.org/10.1016/j.apm.2015.09.094

Sahmani, S., Bahrami, M. and Aghdam, M.M. (2016), "Surface stress effects on the nonlinear postbuckling characteristics of geometrically imperfect cylindrical nanoshells subjected to torsional load", *Compos. Part B Eng.*, **84**, 140-154. https://doi.org/10.1016/j.compositesb.2015.08.076

Son, L.T., Vinh, P.V., Chinh, N.V. and Sedighi, H.M. (2025), "High-frequency temperature-dependent vibration of nonlocal functionally graded sandwich nanoplates resting on elastic foundations", **32**(5), 957-978. https://doi.org/10.1080/15376494.2024.2358108

Su, Y., Zhu, J., Long, X., Zhao, L., Chen, C. and Liu, C. (2023), "Statistical effects of pore features on mechanical properties and fracture behaviors of heterogeneous random porous materials by phase-field modeling", *Int. J. Solids Struct.*, **264**, 112098. https://doi.org/10.1016/j.ijsolstr.2022.112098

Temel, B., Calim, F.F. and Tütüncü, N. (2004), "Quasi-static and dynamic response of viscoelastic helical rods", *J. Sound Vib.*, **271**(3), 921-935. https://doi.org/10.1016/S0022-460X(03)00760-0

Thang, P.T., Do, D.T.T., Lee, J. and Nguyen-Thoi, T. (2023), "Size-dependent analysis of functionally graded carbon nanotube-reinforced composite nanoshells with double curvature based on nonlocal strain gradient theory", *Eng. Comput.*, **39**(1), 109-128. https://doi.org/10.1007/s00366-021-01517-1

Türker, H.T., Cuma, Y.C. and Calim, F.F. (2023), "An efficient approach for free vibration behaviour of non-uniform and non-homogeneous Helices", *IJST-T Cvil. Eng.*, **47**(4), 1959-1970. https://doi.org/10.1007/s40996-023-01075-0

Vinh, P.V. and Tounsi A. (2022), "Free vibration analysis of functionally graded doubly curved nanoshells using nonlocal first-order shear deformation theory with variable nonlocal parameters", *Thin Wall. Struct.*, **174**, 109084. https://doi.org/10.1016/j.tws.2022.109084

Vinh, P.V., Tounsi, A. and Belarbi, M.O. (2023), "On the nonlocal free vibration analysis of functionally graded porous doubly curved shallow nanoshells with variable nonlocal parameters", *Eng. Comput.*, **39**(1), 835-855. https://doi.org/10.1007/s00366-022-01687-6

Vinh, P.V. (2025), "A novel modified nonlocal strain gradient theory for comprehensive analysis of functionally graded nano-plates", *Acta Mech.*, **236**, 173-204. https://doi.org/10.1007/s00707-024-04131-6

Vinh, P.V. and Zenkour, A.M. (2025), "Vibration analysis of functionally graded sandwich porous plates with arbitrary boundary conditions: A new general viscoelastic Winkler-Pasternak foundation approach", *Eng. Comput.*, 1-29. https://doi.org/10.1007/s00366-025-02106-2.

Wang, S., Ding, W., Li, Z., Xu, B., Zhai, C., Kang, W., Yang, W. and Li, Y. (2023), "A size-dependent quasi-3D model for bending and buckling of porous functionally graded curved nanobeam", *Int. J. Eng. Sci*, **193**, 103962. https://doi.org/10.1016/j.ijengsci.2023.103962

Xu, X., Shahsavari, D. and Karami, B. (2021), "On the forced mechanics of doubly-curved nanoshell", *Int. J. Eng. Sci*, **168**, 103538. https://doi.org/10.1016/j.ijengsci.2021.103538

Yang, Q., Zeng, X., Guo, K., Cao, S., Wei, K., Shan, W. and Tamura, Y. (2025), "Analysis of vortex-induced vibration in flexible risers using a physically-meaningful wake-oscillator model", *Eng. Struct.*, **325**, 119415. https://doi.org/10.1016/j.engstruct.2024.119415

Zaoui, F.Z., Ouinas, D. and Tounsi, A. (2019), "New 2D and quasi-3D shear deformation theories for free vibration of functionally graded plates on elastic foundations", *Compos. Part B Eng.*, **159**, 231-247. https://doi.org/10.1016/j.compositesb.2018.09.051

Zhang, X., Shen, S., Luo, Y., Elmaimouni, L. and Yu, J. (2025a), "Dispersion and attenuation characteristics of Lamb waves in multilayered piezoelectric semiconductor plates with imperfect interfaces", *MAMS*, 1-14. https://doi.org/10.1080/15376494.2025.2456681

Zhang, Y., Xu, L., Wang, J., Pan, H., Dou, M., Teng, Y., Fu, X., Liu, Z., Huang, X. and Wang, M. (2025b), "Bagasse-based porous flower-like MoS2/carbon composites for efficient micro-wave absorption", *Carbon Lett.*, **35**, 145-160. https://doi.org/10.1007/s42823-024-00832-z

Zhao, L.C., Tang, M., Zhang, Q.H., Hu, Z.Y., Gao, H.W., Liao, X.Y., Wang, G. and Leng, J. (2018), "Fabrication of a porous metal-organic framework with polar channels for 5-Fu delivery and inhibiting human osteosarcoma cells", *J. Chem.*, 1523154. https://doi.org/10.1155/2018/1523154

CC